Article no. 37

THE CIVIL ENGINEERING JOURNAL 4-2017

DESIGN OF AN ACTIVE LOW FREQUENCY VIBRATION ISOLATION SYSTEM FOR ATOM INTERFEROMETRY BY USING SLIDING MODE CONTROL

*Dong-Yun Luo, Bing Cheng, Bin Wu, Xiao-Long Wang, and Qiang Lin**

Center for Optics and Optoelectronics Research, College of Science, Zhejiang University of Technology, Hangzhou, China, email: g20158028@xs.ustb.edu.cn

ABSTRACT

Active vibration isolation is gaining increased attention in the ultra-high precision application of atom interferometry to effectively treat the unavoidable ground vibration. In this system, a digital control subsystem is used to process and feedback the vibration measured by a seismometer. A voice coil actuator is used to control and cancel the motion of a commercial passive vibration isolation platform. The system level simulation model is established by Simulink software, The simulation results demonstrate the asymptotic stability of the system and the robustness of the control algorithm. Compared with the conventional lead–lag compensation type controller, the algorithm adopted uses sliding mode control, taking advantage of its easy computer implementation and its robust high performance properties. With the feedback path closed, the system acts like a spring system with a natural resonance frequency of 0.02 Hz. The vibration noise in the vertical direction is about 20 times reduced during 0.1 and 2 Hz, The experimental results verify that the isolator has significant vibration isolation performance, and it is very suitable for applications in high precision gravity measurement.

KEYWORDS

Active vibration isolation, Low frequency vibration, Sliding control, Atom interferometry

INTRODUCTION

Ultra-low frequency vibration isolation has valuable applications in precision instruments such as laser interferometers, atomic force microscope, electron-beam microscopes and so on. Similarly, in our precision atom interferometry measurements which have been one of the best items of equipment to measure gravitational acceleration g. Any change in the relative paths of the two Raman beams due to vibrations will be seen as a spurious interferometer phase shift and noise in the measurement. This phase noise directly couples into the interferometer phase and completely washes out the interferometer fringes for longer pulse separations if not addressed[1]. For example, in the 5m atom interferometer(AI), the free evolution time T, can reach 0.8Hz greatly influences the experiment. Therefore, to suppress the low frequency noise primarily caused by the vibration of a retro-reflecting mirror mounted at the bottom of our AI. To prevent the interferometer fringes from washing out, vibrations have to be reduced to a level where the resulting phase shifts are much smaller than 1 rad. Appropriate vibration isolation of the retro-reflecting mirror is crucial for achieving clean atom interferometer fringes at long pulse separation. Constructing a vibration isolation platform capable of delivering sufficient performance has been the main task of this work and is described extensively in the paper.

Chu's team first constructed a system that isolates a key element of our experimental setup from vertical motions of the ground and the surrounding apparatus [1]. The system combines the

passive isolation of mechanical springs and an optical table floating on compressed air with an active system that measures the acceleration of the mass to be isolated and feeds back to a solenoid actuator to cancel this motion [2]. With the feedback path closed, the system acts like a spring-mass system with a natural resonance frequency of 0.033 Hz. The acceleration error signal is reduced from 0.1 to 20 Hz. Freier simplified the structure of his active vibration isolation lowering the effective resonance frequency from 0:5 Hz to 0:025 Hz by exerting an additional force to the payload mass and suppressed the vibrational noise from about 0.03 to 5 Hz by a factor of up to 200.The vibration of the power spectral density stays on a roughly constant value of $1\times10^{-7}\,g/\sqrt{Hz}$ between 0:03 Hz and 0.5 Hz[3]. The accuracy of the existing setup has been improved significantly from $3\times10^{-6}g$ to $5\times10^{-8}g$ .Tang suppress the vertical vibration (0.1–10 Hz) measured by the in-loop seismometer is reduced by an additional factor of up to 500 on the basis of a passive vibration isolation platform.

The teams above mentioned used programs to measure the open-loop frequency response and to graphically set the parameters for the feedback lead–lag compensation filters. They got the highest possible feedback gain of the system with enough phase margin by adjusting the parameters of the feedback filters which is designed by using a combination of lag compensators. The combination of lag compensators contains multiple tuning parameters. For the sake of initial turn-on spike in Ref. [3] .The gain of feedback loop set to the designed value must be slowly increased to its final value over a period of about 3 mins [3]. To deal with these drawback, sliding control strategy which has the advantage of a simple structure, model-free, higher computation efficiency ability and few tuning parameters.We have designed and implemented an active system that combines relatively short mechanical springs with an electronic feedback loop to produce an almost critically damped spring-mass system with an effective resonance frequency of 0.02 Hz by using sliding mode control, thus significantly reducing the effect of harmful vibrations at frequencies from 0.05 to 10Hz [4-5].

THEORY

(1) Vibration Noise

The acceleration of the retro-reflector is indistinguishable for the gravimeter which can measure the gravitational acceleration by the equivalent principle. So the vibration noise has been is the largest noise source of the atomic interferometer, the effect of vibration noise suppression determines the performance of gravity acceleration measurement [6]. The sensitivity of the vibration acceleration function can be expressed as $g_a(t)$:

$$g_a(t)=2\lim_{\delta_a\to0}\frac{\delta P_a(\delta_a,t)}{\delta_a} \tag{1}$$

Where δ_a is an infinitesimal disturbance, $g_s(t)$ is the sensitivity function of the gravimeter, the relationship between $g_a(t)$ and $g_s(t)$ can be expressed as:

$$g_s(t)=\frac{d^2g_a(t)}{k_{eff}dt^2} \tag{2}$$

Where k_{eff} is Raman wave number. The relationship between the vibration acceleration transfer function $H_a(w)$ and the interferometer transfer function $H_\phi(w)$ can be expressed as:

$$\left|H_a(w)\right|^2=\frac{k^2{}_{eff}}{w^4}\left|H_\phi(w)\right|^2 \tag{3}$$

Assume that the power spectral densities of the vibration displacement and the vibration acceleration respectively are $S_Z(w)$ and $S_a(w)$,the power spectral density of the phase $S_\phi(w)$ can be expressed as:

$$S_\phi(w) = \left|k_{eff}\right|^2 S_Z(w) = \frac{\left|k_{eff}\right|^2}{w^4} S_a(w) \tag{4}$$

The rms(root mean square) value of the total phase of the interferometer can be expressed as:

$$(\sigma_\varphi^{\ rms})^2 = \int_0^\infty \left|H_\varphi(w)\right|^2 S_\varphi(w) dw \tag{5}$$

The acceleration transfer function is a low-pass filter effect, the filter cut off rate is $1/(2T)$. With the experimental parameters $T = 70ms$ and $\tau = 4\mu s$, $H_a(f)$ can be expressed as:

$$H(f) = \frac{4}{1-(4\tau f)^2} \sin(\pi(T+2\tau) f)(\sin(\pi T f) + 4\tau f \cos(\pi(T+2\tau) f)) \tag{6}$$

From Figure 1 we can see low frequency vibration has more weight coefficient than high frequency vibration. The surrounding vehicle movement, construction activities around our laboratory have a great impact on interferometer [7-8]. The function of gravity acceleration g measured by interferometer can be expressed as:

$$g = \frac{1}{k_{eff} T^2} \Delta\phi \tag{7}$$

where $\Delta\phi$ is the phase of the interferometer. In order to assess the effect of vibration on the phase, we have mounted retro-reflector mirror on passive isolation platform and measured noise power spectrum which can calculate the contribution of vibration noise under different T.

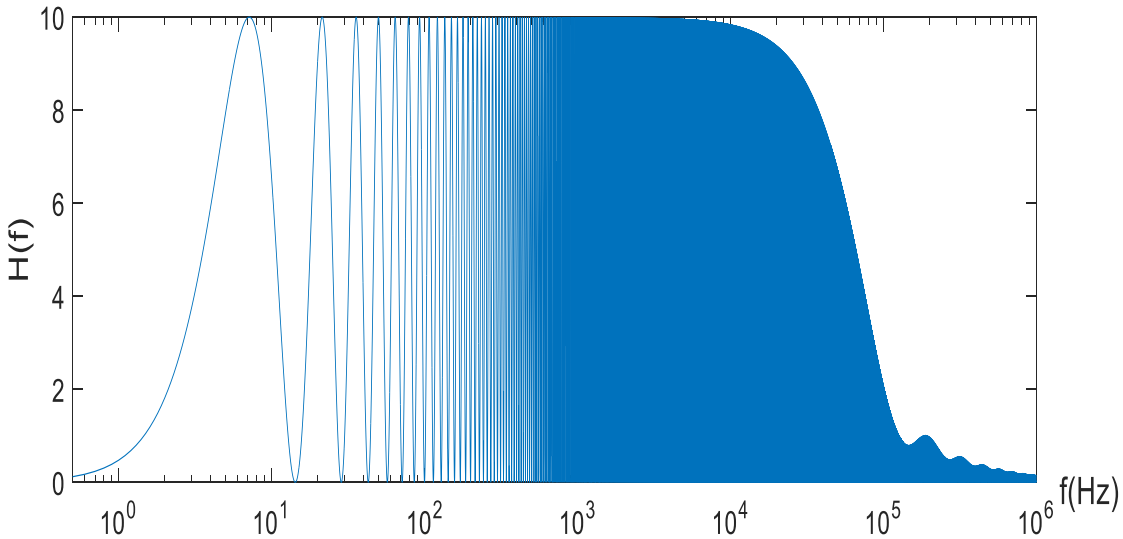

Fig.1 - Weight function curve of influence of Phase Noise on Interferometer Phase

Tab. 1 - Contribution of vibration noise under different T

T （ms）	phase of the interferometer $(mrad)$
40	18.2
50	25.0
60	32.5
70	42.2

(2) Mechanical system

A typical schematic diagram of active vibration isolation is shown in Figure 2. Motion from the ground passing through the spring and damping system drives the mass. A sensor detects the motion of the mass and feedback it to an actuator to generate an equal force in the opposite direction to cancel the motion of the mass [9].

The mechanical setup is based on a commercial passive isolation platform. (25BM-4, Minus K Technology, Inglewood, CA, USA). It has a net payload of 4.5 kg to 10 kg and is easily transportable with dimensions of approx. $31\times31\times11.7cm$ and a weight of 9 kg. By employing patented mechanism using negative stiffness elements, it provides vibration isolation in 3 spatial directions with a low vertical resonance frequency of 0:5 Hz and a horizontal resonance frequency of 1:5 Hz. It is clear that passive vibration isolators can only isolate against ground motions at frequencies above 0:7Hz. There is no effect for vibration below 0.5 Hz. A broadband and sensitive commercial seismometer (CMG-3ESPC) is installed on the top of the passive isolator [10-11]. The seismometer is a triaxial sensor, and can directly measure the velocity of the platform caused by ground vibration. It can measure very low frequency velocity from 0.017 to 50 Hz with sensitivity of $2040V/ms^{-2}$ and a noise level lower than $10^{-9}g/\sqrt{Hz}$, The maximum peak-to-peak value of the differential output voltage of the seismometer is $\pm10V$ [12-15].The voltage signalfrom the seismometer is collected by a FPGA based data acquisition and processing card (NI-9223, National Instruments Corporation, Austin, TX, USA) which is 16-bit resolution.

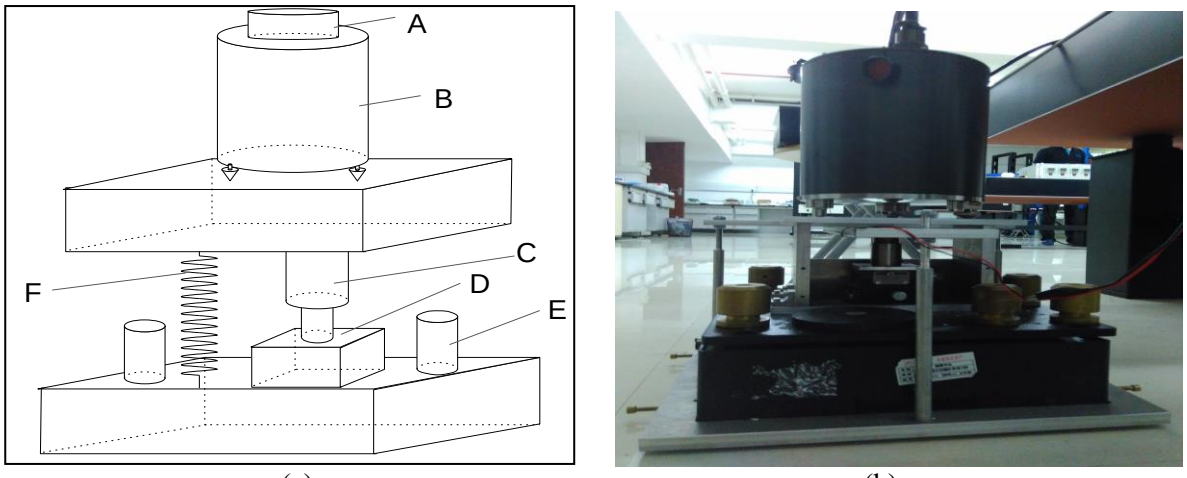

(a) (b)

Fig.2 - (a) and (b) Mechanical setup of our active VIS.(A)mirror, (B)seismometer, (C) voice coil motor, (D) translation stage, (E) counter weight, (F)passive vibration isolation platform

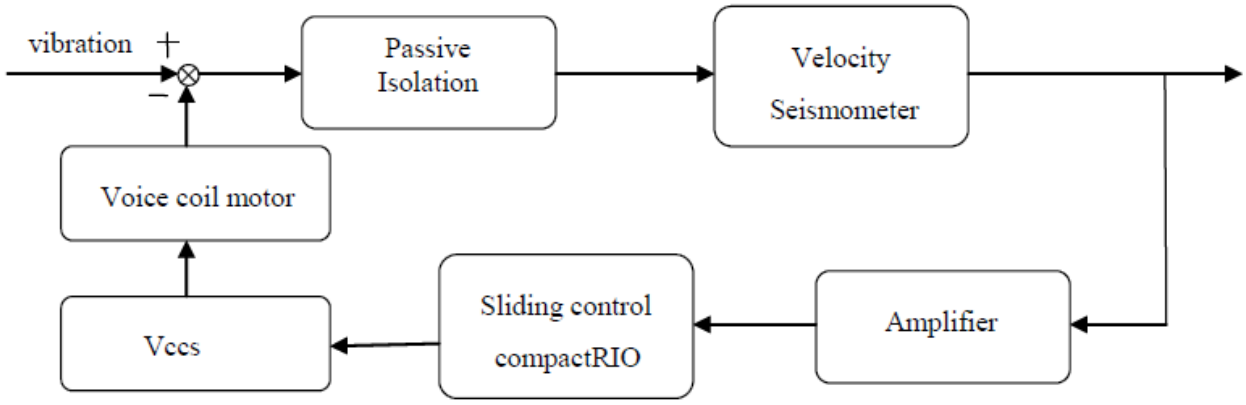

Fig.3 - Diagram of the feedback loop

The acquisition and processing card can only resolve the vibration velocity signal of $1.5\times10^{-7} m/s$,but vibration speed goal is $6.28\times10^{-8} m/s$, so the velocity signals from the sensor are amplified by independent low-noise amplifiers(AD624) which pin programmable gains of 1,200,500 and 1000 can be provided on the chip.We used a National Instruments compactRIO Real-Time Computer System (NI cRIO9031, National Instruments Corporation,Austin, TX, USA) with an FPGA backplane to perform the sliding mode control. All programs were written in NI LabVIEW 2016, The system is controlled remotely via LabVIEW which allows easy access from the main control computer of the atom interferometer. The program running on the FPGA chip and a control and monitoring program implemented on a 1.33GHz CPU which is also part of the cRIO system. The driven current for the voice-coil comes directly from a voltage controlled-current-source (VCCS). The VCCS can provide a current of 500 mA with 5 V driving voltage. The frequency response of the VCCS will limit the bandwidth of the feedback loop. The corner frequency of the VCCS circuits is larger than 100 Hz, while the demand for our feedback loop is only 50 Hz, thus the bandwidth is large enough. Due to size restrictions inside the vertical vibration isolator, small actuators (LA12-17, BEI Technologies, San Marcos, CA, USA) manufactured with a diameter of 30.48mm and a mid-stroke length of 43.18mm were chosen. Because the clearance on each side of voice coil actuator is 0.38 mm, the coil side is mounted on a two-dimensional translation stage, which is used to adjust the space between the coil and magnet [16-18]. The magnet side is mounted on an aluminum plate as shown in Figure 2. A copper coil and magnet s of voice-coil type actuators, each comprised of a copper coil and magnet, are used to provide feedback forces. The force constant is 7.46 N/A, which is obtained by measuring the excited acceleration under a constant driving current. Diagram of the feedback loop is shown in Figure 3.

A mass m whose motion x we wish to decouple from any motion of the ground y is suspended from a spring with linear spring constant k and damping factor c (Figure 1). By analyzing the system we get a well known linear 2nd order dynamic equat ion with constant coefficients [19-21]:

$$\ddot{x} + 2\xi_0\omega_0(\dot{x} - \dot{y}) + \omega_0^{\,2}(x - y) = \frac{F}{x} \qquad (8)$$

Where $\omega_0 = \sqrt{k/m}$ is the intrinsic resonance frequency, $\xi_0 = c/2m\omega_0$ is the intrinsic damping constant, $F = -2mH\dot{x}$, H is the adjustable gain factor of feedback force magnitude. The transfer function of this active system is obtained by Laplace transformation to both sides of Equation 6:

$$\frac{\dot{x}}{\dot{y}} = \frac{2\xi_0\omega_0(i\omega) + \omega_0^{\,2}}{(i\omega)^2 + 2\omega_0(\xi_0 + H)(i\omega) + \omega_0^{\,2}} \tag{9}$$

Equation 8 shows that with the increase in feedback gain H which lower the effective resonance frequency and thus increase the range over which the system tends to isolate motions of the ground from motions of the mass [22-23].

We use signal generator ((DGU1022, RIGOL Corporation, Beijing, China) to produce the frequency swept slowly from 0.03 to 300 Hz to make sure that the data acquisition (DAQ) card obtains enough velocity response data of the platform to calculate its transmissibility. From Figure 4 and Figure 5 we can calculate that $\omega_0 = 2\pi \times 0.7 = 4.396$ and $\xi_0 = 0.1$.

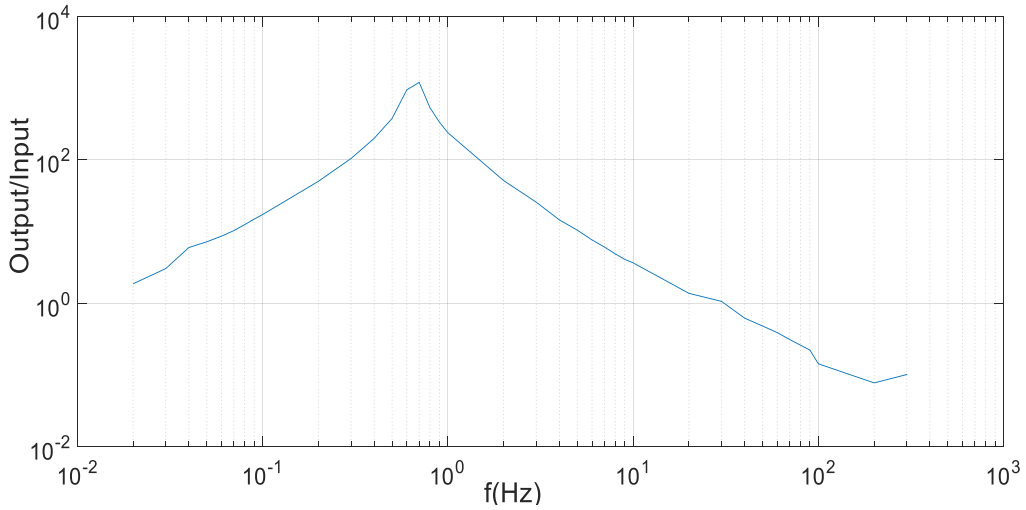

Fig. 4 - Magnitude bode plot of open loop

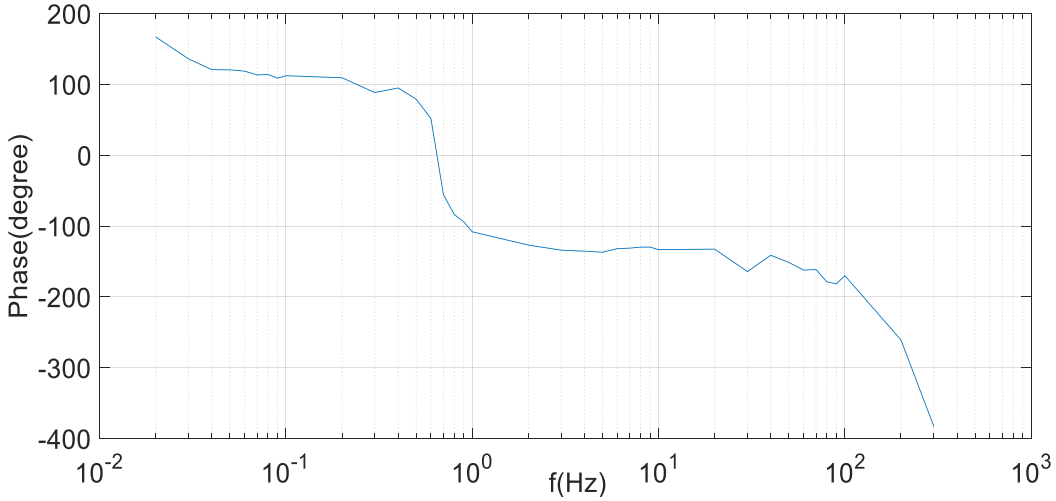

Fig. 5 - Phase bode plot of open loop

SLIDING MODE CONTROL ALGORITHM

(1) Controller Design

From Equation 9 we can deduce active vibration isolation system mathematical model:

$$\ddot{x} + a\dot{x} + lx + bu + d = 0 \tag{10}$$

Where $a = 2\xi_0\omega_0, l = \omega_0{}^2, b = -\frac{1}{m}, d = -2\xi_0\omega_0\dot{y} - \omega_0{}^2 y, F = ku$, u is sliding controller output voltage, d is external disturbance,. d is coefficient between the force of voice coil motor and controller output voltage [24-26].

Sliding surface can be designed as:

$$s(t) = ce(t) + \dot{e}(t) \tag{11}$$

Where $c > 0$,meet Hurwitz condition.Error and its derivative can be expressed as:

$$e(t) = x_d - x \tag{12}$$

$$\dot{e}(t) = \dot{x}_d - \dot{x} \tag{13}$$

Where $x_d = 0$ is the setpoint of the vibration displacement, $\dot{x}_d = 0$ is the setpoint of the vibration velocity,thus:

$$\dot{s}(t) = c\dot{e}(t) + \ddot{e}(t) = c(\dot{x}_d - \dot{x}) + (\ddot{x}_d - \ddot{x}) \tag{14}$$

Substituting Equation (10) into Equation (14) , the following can be achieved:

$$\dot{s}(t) = c(-\dot{x}) + (-a\dot{x} - cx - bu - d) = -(c+a)\dot{x} - cx - bu - d \tag{15}$$

Index approaching law can be designed as:

$$\dot{s}(t) = -\varepsilon\,\mathrm{sgn}(s) - ks \tag{16}$$

Where $\varepsilon > 0, k > 0$.

Equation 15 and Equation 16 can be achieved: $-(c+a)\dot{x} - cx - bu - d = -\varepsilon\,\mathrm{sgn}(s) - ks$

$\mathrm{sgn}(s)$ can be described as:

$$\text{Where } \mathrm{sgn}(s) = \begin{cases} 1 & x > 0 \\ 0 & x = 0 \\ -1 & x < 0 \end{cases}$$

Sliding mode control law can be expressed as:

$$u = \frac{1}{b}[-(c+a)\dot{x} - cx + \varepsilon\,\mathrm{sgn}(s) + ks - d] \tag{17}$$

Obviously,disturbance d is unkown, The above control law can not be achieved, we used disturbance bound to design control law in order to solve this problem [27-28].

Sliding mode control law can be designed as:

$$\dot{s}(t) = c(-\dot{x}) + (-a\dot{x} - cx - bu - d) = -(c+a)\dot{x} - cx - bu - d \tag{18}$$

Where d_c is positive real number related to disturbance d bound.

Substituting Equation 18 into Equation 15 , the following can be achieved:

$$u = \frac{1}{b}[-(c+a)\dot{x} - cx + \varepsilon \operatorname{sgn}(s) + ks - d_c] \tag{19}$$

The stability of the control system is ensured by selecting d_c ,satisfy the sliding mode arrival condition,assume: $d_L \le d \le d_U$ (20)

Where d_L and d_U are disturbance bound.

$$d_c = d_2 - d_1 \operatorname{sgn} s \tag{21}$$

Where $d_1 = \frac{d_U - d_L}{2}$ and $d_2 = \frac{d_U + d_L}{2}$

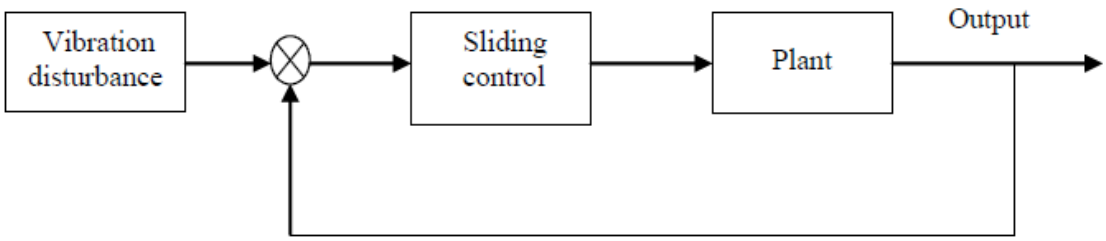

Fig. 6 - Diagram of the Sliding control

(2) Simulation

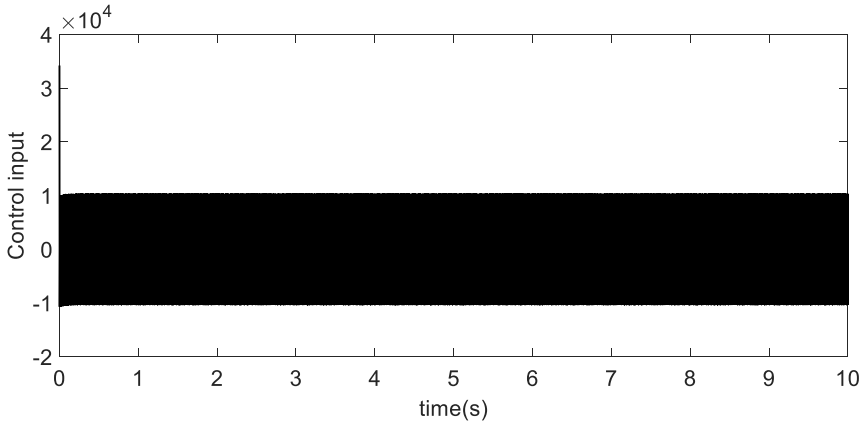

Fig. 7 - Sliding controller output

Figure 7 shows the control input for sliding controller. As can be seen, the control input of sliding controller shows continuous fluctuations. This is because the rule bank changes with each sampling point, and the continuous switching back and forth produces this chattering. By injecting a sinusoidal signal into the system (Figure 8),one can also observe that the control is effective in suppressing vibrations. Acceleration in z is reduced from 1 to 10^{-6}.Overall, the sliding controller is better than the lead–lag controller; it has better vibration isolation effect.

Tab 2. - Values of control parameters used in Sliding control

Symbol	Description	Properties	Unit
ω_0	natural resonance frequency	4.396	rad…
ξ_0	natural damping constant	0.1	N/(m/s)
m	Weight of load	10	Kg
c	Sliding surface coefficient	15	
d_U	Upper bound	26	
d_L	Lower bound	-26	
ε	exponential approach law coefficient	1000	
k	exponential approach law coefficient	1000	

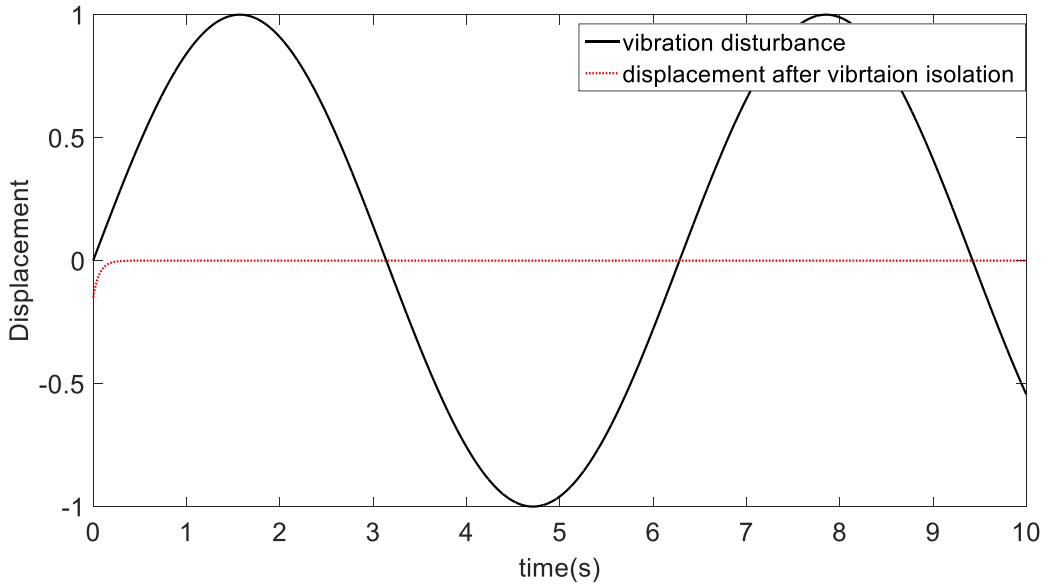

Fig. 8 - Vibration isolation simulation results of sliding controller

(3) Experiment Results

The performances of our active vibration isolation are shown in Figure 9. Figure 9 shows that the vibrational noise around 0.8 Hz has been suppressed by up to 300 times when the feedback is turned on with in loop measurement. The actual bandwidth of in-loop measurement was 0.08–10 Hz, which matched the theoretical prediction. Maximum vibration suppression is higher than 300 at the intrinsic resonant frequency of the passive system, and the vibration of 0.08–0.1 Hz was reduced by a factor of 3, while the vibration of 0.1–3 Hz was reduced by a factor of more than 50.

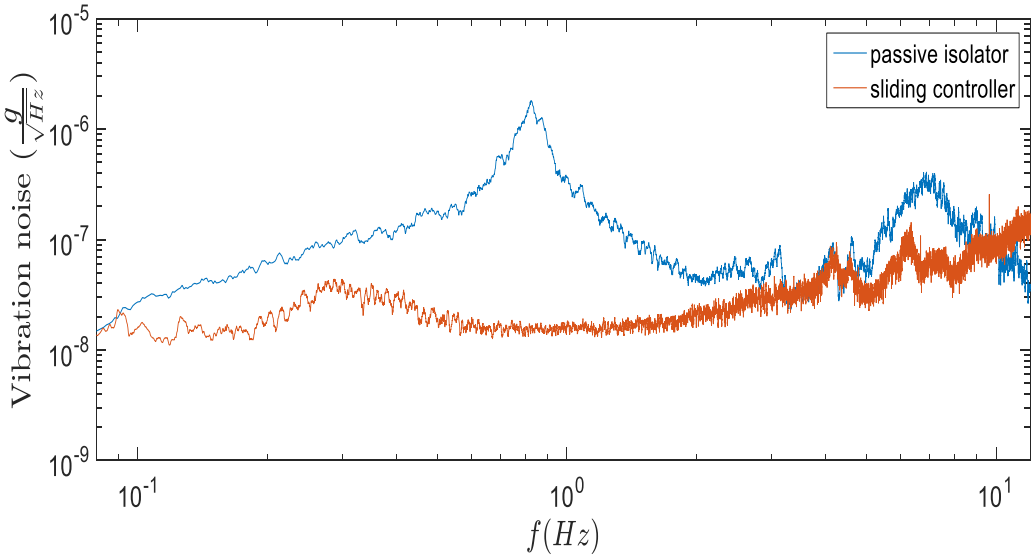

Fig. 9 - The performance of our active vibration isolation

The interference fringe of T = 60 ms is obtained by varying the chirp rate, which is displayed in Figure 11. The phase measurement of the fringe is obtained with a sinusoidal fit of the experimental data. The total interrogation time is optimized to 120ms and repetition rate is 2.2 Hz. The number of total points is 57 and each point is obtained as an average of four times; one full fringe period corresponds to 102 s.

CONCLUSIONS

We have implemented this active vertical vibration isolation system, by comparing the error signal reduction of our single-stage vertical vibration isolation system with the reported isolation of with the lowest effective resonance frequency. Maximum vibration suppression is higher than 300 at the intrinsic resonant frequency of the passive system, and the vibration of 0.08–0.1 Hz was reduced by a factor of 3, while the vibration of 0.1–3 Hz was reduced by a factor of more than 50.Despite a short total interrogation time of 120 ms, a sensitivity of $1.0\times10^{-7}\,g/\sqrt{Hz}$ and a resolution of $5.7\times10^{-9}\,g$ within 1000 s integration time were achieved. The long-term gravity data of 128 h were measured and they are in good agreement with the standard tidal model. In addition, a seismic wave of about 1h has been recorded by our atomic gravimeter.

ACKNOWLEDGEMENTS

This study was supported by the National Natural Science Foundation of China (Grant Nos. 61475139) and National Basic Research Program of China (973 Program-2013CB329501).Our gratitude is also extended to reviewers for their efforts in reviewing the manuscript and their very encouraging, insightful and constructive comments.

REFERENCES

[1] Hensley, J. M., et al. (1999). "Active low frequency vertical vibration isolation." Review of Scientific Instruments, 70(6): 2735-2741.

[2] Zhou, M. K., et al. (2015). "Note: A three-dimension active vibration isolator for precision atom gravimeters." Review of Scientific Instruments, 86(4): 046-108.

[3] Tang, B., et al. (2014). "A programmable broadband low frequency active vibration isolation system for atom interferometry." Review of Scientific Instruments, 85(9): 093-109.
[4] Wang wen-chao., et al.(2010)."Design and Matlab simulation of an ultra-low frequency vibration-isolating system for atom interferometers." Chinese Journal of Quantum Electronics, 27(3): 367-372.
[5] Tjepkema, D., et al. (2012)."Sensor fusion for active vibration isolation in precision equipment." Journal of Sound and Vibration,331(4): 735-749.
[6] Boulandet, R., et al. (2016)."A sensorless method for measuring the point mobility of mechanical structures." Journal of Sound and Vibration, 378: 14-27.
[7] Tang, B., et al.(2014). "A programmable broadband low frequency active vibration isolation system for atom interferometry." Review of Scientific Instruments, 85(9): 093-109.
[8] Fu, J., et al. (2016)."Model-free fuzzy control of a magnetorheological elastomer vibration isolation system: analysis and experimental evaluation." Smart Materials and Structures, 25(3): 035030.
[9] Ahmad Mazlan, A. Z. and Z.Mohd Ripin (2017). "The effective frequency range of an active suspended handle based on the saturation effects of a piezo stack actuator." Journal of Vibration and Control, 23(5): 752-769.
[10] Aloufi, B., et al. (2016)."Modeling and design of a high-performance hybrid actuator." Smart Materials and Structures, 25(12): 125004.
[11] Liang, J. W., et al. (2013)."Active suppression of pneumatic vibration isolators using adaptive sliding controller with self-tuning fuzzy compensation." Journal of Vibration and Control, 21(2): 246-259.
[12] Yen, J.-Y., et al. (2005)."Active vibration isolation of a large stroke scanning probe microscope by using discrete sliding mode control." Sensors and Actuators A: Physical, 121(1): 243-250.
[13] Li, B., et al.(2014). "Dynamic modeling and control for a five-dimensional hybrid vibration isolator based on a position/orientation decoupled parallel mechanism." Journal of Vibration and Control ,22(15): 3368-3383.
[14] Hogsberg, J. and M. L. Brodersen (2014). "Hybrid viscous damper with filtered integral force feedback control." Journal of Vibration and Control 22(6): 1645-1656.
[15] Xia, Z., et al. (2016). "Non-linear dynamic analysis of double-layer semi-active vibration isolation systems using revised Bingham model." Journal of Low Frequency Noise, Vibration and Active Control ,35(1): 17-24.
[16] Li, G., et al.(2014). "Ultra-low frequency vertical vibration isolator based on LaCoste spring linkage." Review of Scientific Instruments, 85(10): 104502.
[17] Kim, M. H., et al. (2016)."Design and Control of a 6-DOF Active Vibration Isolation System Using a Halbach Magnet Array." IEEE/ASME Transactions on Mechatronics 21(4): 2185-2196.
[18] Van de Ridder, L., et al. (2016)."Coriolis mass-flow meter with integrated multi-DOF active vibration isolation." Mechatronics 36: 167-179.
[19] Chen, H. Y., et al. (2013)."Active pneumatic vibration control by using pressure and velocity measurements and adaptive fuzzy sliding-mode controller." Sensors (Basel), 13(7): 8431-8444.
[20] Persson, P., et al. (2016)."Numerical study of reduction in ground vibrations by using barriers." Engineering Structures ,115: 18-27.
[21] Stabile, A., et al.(2017). "Design and verification of a negative resistance electromagnetic shunt damper for spacecraft micro-vibration." Journal of Sound and Vibration, 386: 38-49.
[22] Plattenburg, J., et al. (2016). "A new analytical model for vibration of a cylindrical shell and cardboard liner with focus on interfacial distributed damping." Mechanical Systems and Signal Processing, 75: 176-195.
[23] Sang, H., etal.(2016). "A fuzzy neural network sliding mode controller for vibration suppression in robotically assisted minimally invasive surgery." Int J Med Robot, 12(4): 670-679.
[24] Ning, D., et al. (2016). "Active control of an innovative seat suspension system with acceleration measurement based friction estimation." Journal of Sound and Vibration, 384: 28-44.
[25] Le, T. D.and K. K.Ahn (2013)."Fuzzy sliding mode controller of a pneumatic active isolating system using negative stiffness structure." Journal of Mechanical Science and Technology, 26(12): 3873-3884.
[26] Ouyang, H., et al. (2016). "Load vibration reduction in rotary cranes using robust two-degree-of-freedom control approach." Advances in Mechanical Engineering,8(3): 168781401664181.

[27] Tourajizadeh, H. and S.Zare (2016)."Robust and optimal control of shimmy vibration in aircraft nose landing gear." Aerospace Science and Technology, 50: 1-14.
[28] Oliveira, F., et al.(2015)."A comparative study of semi-active control strategies for base isolated buildings." Earthquake Engineering and Engineering Vibration, 14(3): 487-502